FRONTIERS OF PHYSICS

RESEARCH ARTICLE
Volume 19 / Issue 3 / 33209 / 2024

Optimization for epitaxial fabrication of infinite-layer nickelate superconductors

Minghui Xu[1,*], Yan Zhao[1,*], Xiang Ding[1], Huaqian Leng[1], Shu Zhang[1], Jie Gong[1], Haiyan Xiao[1], Xiaotao Zu[1], Huiqian Luo[4,5], Ke-Jin Zhou[3], Bing Huang[2], Liang Qiao[1,†]

1 School of Physics, University of Electronic Science and Technology of China, Chengdu 610054, China
2 Beijing Computational Science Research Center, Beijing 100193, China
3 Diamond Light Source, Harwell Campus, Didcot OX11 0DE, United Kingdom
4 Beijing National Laboratory for Condensed Matter Physics, Institute of Physics, Chinese Academy of Sciences, Beijing 100190, China
5 Songshan Lake Materials Laboratory, Dongguan 523808, China
*These authors contributed equally to this work.
Corresponding author. E-mail: †liang.qiao@uestc.edu.cn
Received July 5, 2023; accepted November 5, 2023

ABSTRACT

The discovery of nickelates superconductor creates exciting opportunities to unconventional superconductivity. However, its synthesis is challenging and only a few groups worldwide can obtain samples with zero-resistance. This problem becomes the major barrier for this field. From plume dynamics perspective, we found the synthesis of superconducting nickelates is a complex process and the challenge is twofold, i.e., how to stabilize an ideal infinite-layer structure $Nd_{0.8}Sr_{0.2}NiO_2$, and then how to make $Nd_{0.8}Sr_{0.2}NiO_2$ superconducting? The competition between perovskite $Nd_{0.8}Sr_{0.2}NiO_3$ and Ruddlesden–Popper defect phase is crucial for obtaining infinite-layer structure. Due to inequivalent angular distributions of condensate during laser ablation, the laser energy density is critical to obtain phase-pure $Nd_{0.8}Sr_{0.2}NiO_3$. However, for obtaining superconductivity, both laser energy density and substrate temperature are very important. We also demonstrate the superconducting $Nd_{0.8}Sr_{0.2}NiO_2$ epitaxial film is very stable in ambient conditions up to 512 days. Our results provide important insights for fabrication of superconducting infinite-layer nickelates towards future device applications.

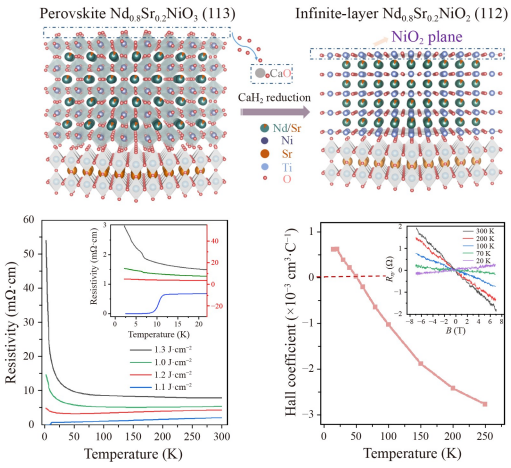

Keywords nickelate superconductivity, infinite-layer, plasma condensate, plume dynamics

1 Introduction

Ever since the discovery of copper-based high-temperature superconductivity, there has been a strong motivation to identify non-cuprates superconductor with similar cuprates-like electronic structures. Considering Ni is next to Cu in the periodic table, there are high expectations to find superconductivity in nickel oxides [1]. Initial attempts in the past three decades turned out to be unsuccessful, until recently, Li *et al.* [2] discovered superconductivity in infinite-layer nickelate $Nd_{0.8}Sr_{0.2}NiO_2$ epitaxial films, leading to a new era for the research of superconductivity. In addition, understanding of the nickel-based superconductivity might

https://doi.org/10.1007/s11467-023-1368-1

provide useful clue to elucidate the superconductivity mechanisms for cuprates and pnictides.

Despite sharing many similarities (i.e., $3d^9$ electronic configuration, hole-doping superconducting phase-diagrams [3, 4], small coherent length [5], weak electron–phonon coupling [6], superconducting dimensionality [5, 7]), nickelates still exhibit some essential differences compared with cuprates. For example, cuprates are mainly charge-transfer insulators with doped holes residing in O 2p orbitals forming Zhang–Rice singlets, while nickelates show Mott–Hubbard-like behavior with doped holes staying in Ni 3d bands. Cuprates show ideal single-band feature, while nickelates show multi-band feature (Ni $3d_{x^2-y^2}$, Ni $3d_{z^2}$, Nd 5d and interstitial orbitals) [8, 9]. Cuprates show higher transition temperature (T_c) with long-range antiferromagnetic ordering, while nickelates show lower T_c and local antiferromagnetic fluctuations. Recently, charge density wave, spin excitation and strong Pauli-limit violation have been identified in infinite-layer nickelates [5, 8, 10–13].

Currently, there are few debates on the physics of infinite-layer nickelates, e.g., intrinsic magnetism (whether long-range or short-range antiferromagnetic ordering) [8, 14–16] and pair mechanism (s-wave, d-wave, or s/d wave) [6, 17–20]. Moreover, nickelates superconductivity is only observed in epitaxial films, not in bulk polycrystalline or single crystals [21]. These issues reflect our understanding of the fundamental properties of infinite-layer nickelates is still limited, which is essentially restricted by the challenge in material synthesis.

The chemical synthesis of infinite-layer nickelate can be traced back to early 1980s. Since then, scientists have been studying to find effective methods for chemical reduction until metal hydrides are proposed as reducing agent [Fig. 1(a)], which can work at relatively low temperatures [22, 23]. This technique is then applied to perform reduction for epitaxial perovskite films (e.g., $LaNiO_3$, $BaTiO_3$, $SrFeO_3$, $SrVO_3$) [24–28] and layered materials (e.g., LaFeAsO, $Sr_3Co_2O_4$, $Sr_3Fe_2O_4Cl_2$, $LaBaCo_2O_5$) [29–32]. Compared with other perovskites, the difficulty of chemical reduction for doped nickelates is twofold: (i) the most stable valence state for Ni is +2, while high valence states (e.g., +3 for $LaNiO_3$ and +3.2 for $Nd_{0.8}Sr_{0.2}NiO_3$) and ultra-low valence state (+1 for $LaNiO_2$) are thermodynamically unstable [23]. (ii) Sr doping decreases the stability for perovskite nickelate, thus secondary phases or structure defects (Ruddlesden–Popper domains) often coexist [33, 34], which is detrimental for achieving superconductivity. Therefore, the synthesis of superconducting nickelate is a great challenge and currently only a few groups worldwide can obtain high-quality superconducting infinite-layer film with zero-resistance [2, 3, 15, 20, 35–38]. This problem becomes the major barrier for the development of this field, thus requires further investigation.

Our group has recently made progress in synthesizing

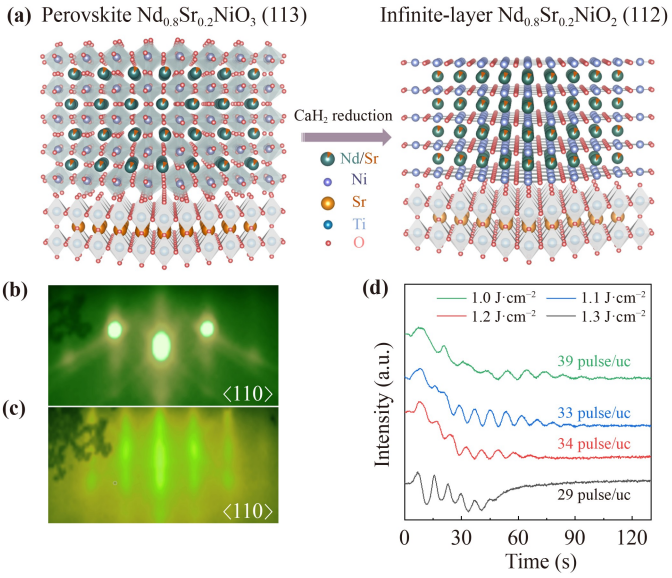

Fig. 1 Growth process for $Nd_{0.8}Sr_{0.2}NiO_3$ thin films. **(a)** Illustration for the CaH_2 topotactic reduction, which can convert perovskite phase into infinite-layer phase. **(b)** RHEED diffraction spot of $SrTiO_3$ (001) observed before growth, and **(c)** RHEED diffraction spot of $Nd_{0.8}Sr_{0.2}NiO_3$/$SrTiO_3$ (001) after growth (1.1 J·cm^{-2}). **(d)** Oscillation curves of the RHEED intensity monitored during the growth of $Nd_{0.8}Sr_{0.2}NiO_3$/$SrTiO_3$ (001) films at different energy densities.

superconducting nickelate epitaxial films [11, 36]. In this work, using 20% Sr-doped neodymium nickelate as an example, we systematically investigate the thin-film growth process during pulsed laser deposition (PLD) from plume dynamics perspective. Through thorough materials characterizations, we show the challenges for obtaining superconducting nickelates involve two key aspects. One is to obtain infinite-layer crystal structure and the other is to achieve ideal superconducting state. In particular, the laser energy density and growth temperature are demonstrated as critical parameters to obtain phase-pure infinite-layer $Nd_{0.8}Sr_{0.2}NiO_2$, which is important to achieve superconducting nickelates. Under optimized growth conditions, $Nd_{0.8}Sr_{0.2}NiO_2$ film exhibits a T_c of 13 K and zero-resistance at 7 K. We also demonstrate that the superconducting $Nd_{0.8}Sr_{0.2}NiO_2$ film is very stable in ambient conditions up to 512 days.

2 Results and discussion

PLD is a well-established technique to grow epitaxial high-quality crystalline materials, particularly for high crystallographic symmetry oxides such as perovskites and spinels [39, 40], for both scientific research and industry applications. A distinguished feature of PLD is the congruent material transfer under ultrafast laser pulses, which enables to grow high-quality films with

complex cation composition [41, 42]. Technically, many instrumental parameters can affect the film growth process, such as substrate temperature, oxygen pressure, laser energy density, laser spot size/uniformity, laser frequency, deposition rate, growth time/film thickness, and substrate-target distances. Practically, the first three parameters are the most important, which deserve systematical study.

For nickelates, synergetic Pauli exclusion principle and Hund coupling enables the d^8 electronic configuration ($t_{2g}^6e_g^2$) to be more energetically stable than others such as d^7 ($t_{2g}^6e_g^1$), d^6 ($t_{2g}^6e_g^0$), or d^9 ($t_{2g}^6e_g^3$), making Ni^{+2} the most favorable valence state for nickel oxides. This is the fundamental reason that nickel monoxide NiO is naturally more common than nickel sesquioxide Ni_2O_3. As a result, to achieve higher Ni valence states, e.g., Ni^{3+} for $LaNiO_3$, high oxygen pressure or ozone is needed to compensate oxygen loss during materials synthesis [43, 44]. Otherwise, oxygen vacancy still dominates, leading to Ni^{2+}/Ni^{3+} mixtures, which masks the intrinsic material properties or physical phenomena [45]. Over the past decades, it is well-established that to ensure high-quality epitaxial $LaNiO_3$ films with minimal oxygen vacancies, high oxygen pressure during film deposition is critical [46, 47]. Considering $Nd_{0.8}Sr_{0.2}NiO_3$ shows even higher Ni valence states ($Ni^{3.2+}$) than $LaNiO_3$ (Ni^{3+}) due to 20% divalent Sr^{2+} doping, we use the highest oxygen pressure of 200 mTorr, which is the limit that can be tolerated by our high-pressure RHEED system. As a result, we narrow down the aforementioned three critical growth parameters into two, i.e., laser energy density and substrate temperature, which will be the focus in the following study.

Although two early studies have considered the film processing conditions for superconducting nickelates [33, 38], the experiments and discussions are not rigorous, i.e., they either did not use the same sample that has been subjected to consecutive growth and reduction processes, or the considered samples are not under the same conditions (i.e., there exists extra variation on film thickness, or cover layer, or reduction parameters), thus these studies are not based on single variation of parameters. In this work, to avoid the similar problem of experiment design and to ensure the accuracy of single variation of parameters, precise film growth rates (under different laser energy density and substrate temperature) are determined by RHEED oscillations and XRR, respectively. Then, all film depositions are performed with calibrated growth rate to ensure identical film thickness for all samples.

Typical RHEED diffraction patterns and intensity oscillations for $Nd_{0.8}Sr_{0.2}NiO_3$ films are first studied. Figures 1(b) and (c) show the representative RHEED spots before and after $Nd_{0.8}Sr_{0.2}NiO_3$ film growth along [110] orientation. The sharp RHEED pattern indicates the film surface after growth is flat. Figure 1(d) shows the RHEED intensity oscillation monitored for the films grown at different laser fluences. The periodic oscillation indicates a typical layer-by-layer growth mode. Note RHEED oscillation during initial growth stage shows nonuniform periodicity, indicating possible existence of surface reconstruction and roughing, which may reflects the competition between the Ruddlesden–Popper phase and the perovskite phase due to comparable formation energy [33].

Figure 2(a) shows XRD scans of 15-nm-thick epitaxial $Nd_{0.8}Sr_{0.2}NiO_3$ films under different laser energy densities (1.0–1.3 J·cm^{-2}). All growth was performed at substrate temperature of 600 °C, oxygen pressure of 200 mTorr and laser frequency of 4 Hz. Generally, all films show well-defined diffraction peaks with clear Kiessig fringes, suggesting good film quality. The left inset in Fig. 2(a) shows the reciprocal space mapping (RSM) of $Nd_{0.8}Sr_{0.2}NiO_3$ film near $SrTiO_3$ (103) reflection, where the film is clamped to $SrTiO_3$ in-plane lattice, indicating a coherent strain state with good epitaxial relationship. The right inset in Fig. 2(a) shows a representative AFM image, indicating the film surface exhibits an atomically smooth step-like structure, further confirming the high-quality perovskite film growth. Note at laser energy density of 1.0 and 1.3 J·cm^{-2}, the film (001) peak is strongly suppressed, indicating Ruddlesden–Popper defective phase [33]. Figure 2(b) shows a zoomed-in XRD near the (002) peak with the inset showing the extracted c lattice parameters. The (002) peak positions show clear laser energy density dependency, e.g., samples at the intermediate energy densities (1.1 and 1.2 J·cm^{-2}) show higher (002) peak positions exceeding 48.4° (c lattice parameter is close to bulk value of 3.75 Å), while samples at the large and small energy densities (1.0 and 1.3 J·cm^{-2}) show low (002) peak positions below 48° with suppressed peak intensity, reflecting dominancy of Ruddlesden–Popper phase [33]. The persistent XRR oscillations in Fig. 2(c) also confirm the flat film surface, consistent with AFM results. The film thickness determined by XRR is also consistent with RHEED oscillations.

The as-grown $Nd_{0.8}Sr_{0.2}NiO_3$ films are then subjected to CaH_2 topotactic reduction at the optimized conditions (300 °C and 2 hours) [11, 36]. The XRD spectra for the reduced films are shown in Fig. 2(d). Note for nonoptimized laser energy densities (1.0 and 1.3 J·cm^{-2}), the reduced film does not show well-defined (002) peak with weak (001) peak, suggesting the Ruddlesden–Popper phase dominated precursor film cannot be reduced to ideal infinite-layer structure. While for intermediate laser energy densities (1.1 and 1.2 J·cm^{-2}), the samples show well-defined diffraction peak and correct lattice parameters [inset of Fig. 2(e)], indicating the formation of infinite-layer $Nd_{0.8}Sr_{0.2}NiO_2$ films. In addition, under the optimized laser energy density (1.1 J·cm^{-2}), the (001)/(002) peaks show stronger intensity, indicating better crystallinity.

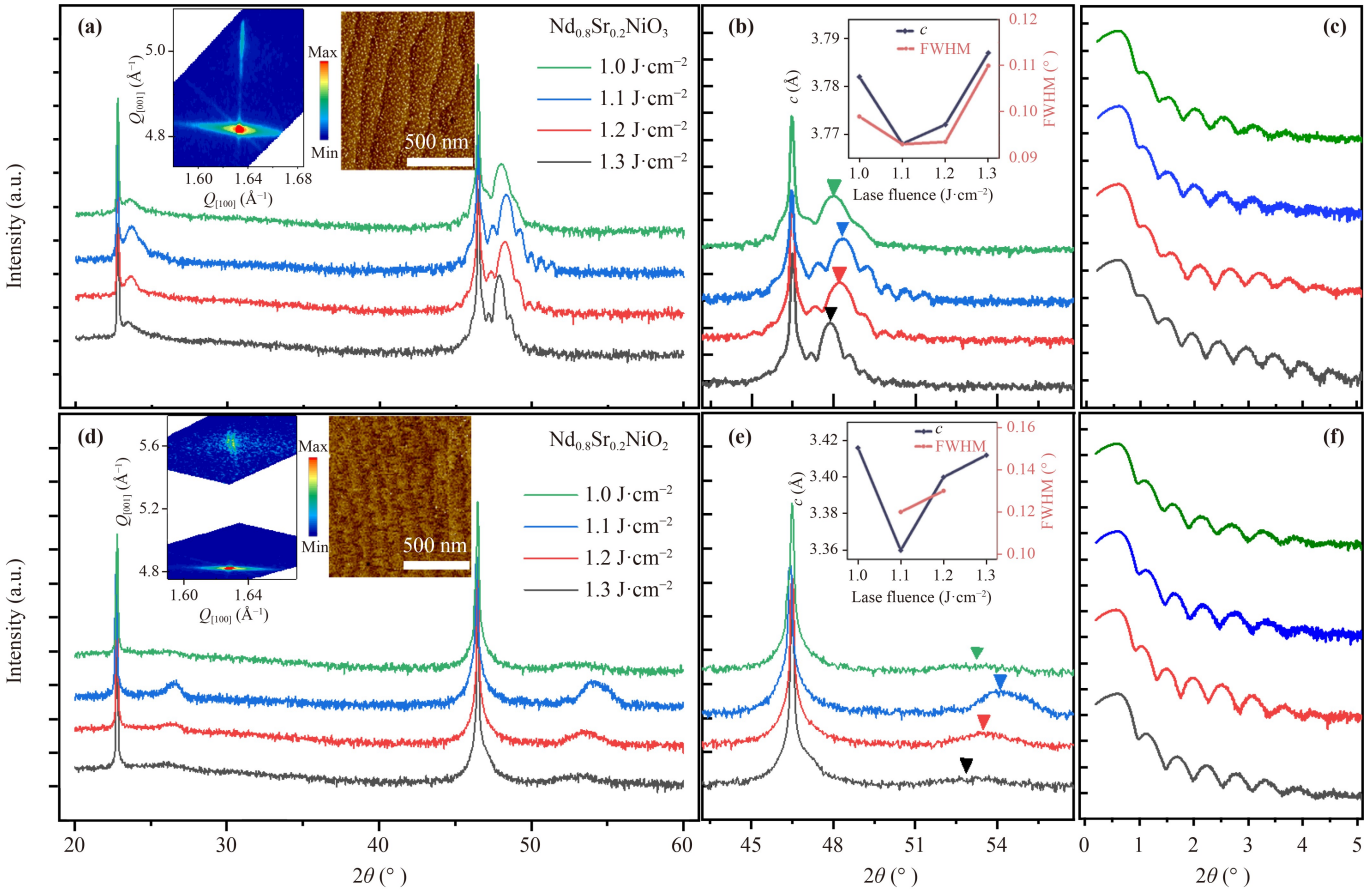

Fig. 2 Effect of laser energy density on the structural characteristics of nickelate thin films. **(a)** X-ray diffraction (XRD) patterns of 15-nm-thick $Nd_{0.8}Sr_{0.2}NiO_3$ (001) films grown on single-crystal $SrTiO_3$ (001) substrates using different laser energy densities and **(b)** the zoomed-in view. The inset in (a) shows reciprocal space maps (RSM) of $Nd_{0.8}Sr_{0.2}NiO_3$ (left) around the (103) $SrTiO_3$ diffraction peak and the surface morphology of $Nd_{0.8}Sr_{0.2}NiO_3$ (right) film by atomic force microscopy (AFM). The inset in (b) shows rocking curve FWHM values and *c*-axis lattice constants recorded for the (002) peak from $Nd_{0.8}Sr_{0.2}NiO_3$ films grown as functions of energy laser. **(c)** Measured XRR of as-grown $Nd_{0.8}Sr_{0.2}NiO_3$. **(d)** The XRD pattern of $Nd_{0.8}Sr_{0.2}NiO_2$ film after reduction corresponds to the growth conditions in (a). The inset in (d) shows reciprocal space maps (RSM) of $Nd_{0.8}Sr_{0.2}NiO_2$ (left) around the (103) $SrTiO_3$ diffraction peak and the surface morphology of $Nd_{0.8}Sr_{0.2}NiO_2$ (right) film by atomic force microscopy (AFM). **(e)** The zoomed-in view of (d). The inset in (e) shows rocking curve FWHM values and *c*-axis lattice constants recorded for the (002) peak from $Nd_{0.8}Sr_{0.2}NiO_2$ films. **(f)** Measured XRR of as-grown $Nd_{0.8}Sr_{0.2}NiO_2$.

The RSM and AFM [inset of Fig. 2(d)] indicate coherent strain and step-like surface structure, suggesting the obtained $Nd_{0.8}Sr_{0.2}NiO_2$ still maintains well-developed epitaxial relationship after CaH_2 reduction.

To understand the correlation between laser energy density and electrical properties, temperature dependent resistivity was measured down to 1.6 K for all the reduced films [Fig. 3(a)]. Generally, all samples show a similar resistivity trend above 100 K, consistent with literature results [4]. At non-optimized conditions (1.0 and 1.3 J·cm^{-2}), the films after CaH_2 reduction are dominated by the reduced Ruddlesden–Popper phase, thus exhibit metal–insulator transition with large resistance below 100 K. For intermediate condition (1.2 J·cm^{-2}), the reduced film shows a metallic-like behavior, but resistivity upturn still appears below 25 K, suggesting Kondo scattering [4]. In contrast, the $Nd_{0.8}Sr_{0.2}NiO_2$ film grown at optimized condition (1.1 J·cm^{-2}) demonstrates clear superconducting transition below 13 K and achieves zero-resistance near 7 K. Figure 3(b) illustrates the temperature dependent Hall coefficient (R_H) for the superconducting $Nd_{0.8}Sr_{0.2}NiO_2$ film. At room temperature, the R_H is negative and is large in magnitude, while at low temperatures (~50 K), R_H shows a negative-to-positive sign conversion. These features are generally consistent with hole-doping of an electronic system with multiorbital contributions, suggesting mixed carrier contributions from electrons and holes [3, 4].

Since the electrical data in Fig. 3(a) are from four samples fabricated with identical film growth and reduction parameters (i.e., substrate temperature, oxygen pressure, film thickness, CaH_2 reduction temperature and reduction

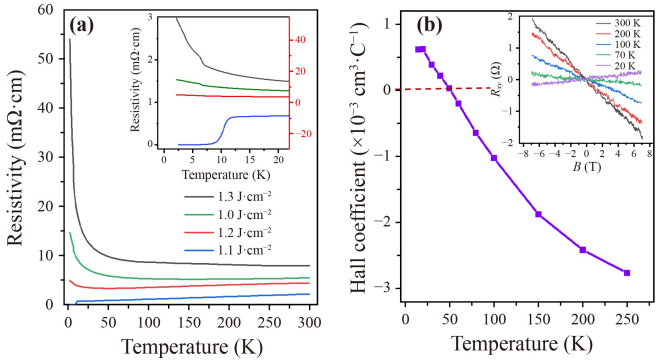

Fig. 3 Effect of laser energy density on transport properties and superconductivity for nickelate thin films after CaH_2 reduction. The data corresponds to the transport characteristic curve of $Nd_{0.8}Sr_{0.2}NiO_2$ films in (d). **(a)** Temperature-dependent resistivity of the CaH_2 reduced $Nd_{0.8}Sr_{0.2}NiO_2$ thin film grown at different laser energy densities. **(b)** The normal Hall coefficient $R_H(T)$ of the superconducting sample in (a).

time) except the only change in laser energy density, these data directly reveal the critical role of laser energy density for the formation of superconducting nickelates. Such a critical dependency leads to a super narrow "growth window" for perovskite precursor $Nd_{0.8}Sr_{0.2}NiO_3$ film, which can be understood from fundamental laser ablation perspective. PLD is not a simple laser-induced thermal melting and vaporization process, but rather complex involving ultrafast ablation and subsequent laser-solids interaction. Typically, the ultrafast (30 ns) excimer laser pulse with a certain energy will be strongly absorbed by oxide target surface (within a depth of few tens of nm) in a confined area of few mm^2 (laser spot). Rapid local heating (~fs) far exceeds thermal relaxation (~μs) leading to an extreme environment with strong deviation from thermodynamic equilibrium limit. As a result, dense plume of plasma condensate will be created, which will be further heated and accelerated by the incoming photons.

This plasma condensate is very important for the formation of epitaxial films with correct phase [48–50]. Although the shape and content of the plasma condensate can be affected by other growth parameters (e.g., oxygen pressure, growth temperature), the laser energy plays the most critical role, as it can directly affect the angular distribution of the elements in the plasma condensate, which is critical for the formation of the materials with correct crystallographic phase [42, 51]. In the past decades, it is found that inequivalent angular distribution of the constitutes (in targets) can lead to significant deviation from the ideal film by forming secondary phase or crystal defects, as demonstrated in complex oxides $LaAlO_3$ [52, 53], $YBa_2Cu_3O_{7-x}$ [54], $SrTiO_3$ [55], $SrZrO_3$, [56] $(Pr,Sr)MnO_3$ [57], and $Pb(Zr,Ti)O_3$ [58]. Likewise, the large atomic mass mismatches between Nd and Ni as well as the natural volatility of nickel oxide turn $(Nd,Sr)NiO_3$ to be a complex system with inequivalent angular distribution of plume condensate during PLD. This hidden plume dynamics issue, together with low formation energy of Ruddlesden–Popper secondary phase, makes the formation of perovskite $(Nd,Sr)NiO_3$ to be very challenging with rather narrow "growth window" and laser energy density is the most critical growth parameter. Furthermore, the nominal laser energy density might be slightly different from the actual laser energy density due to variation of uniformity/focus of the laser beam and laser-induced morphological modification at target surface. Thus, the optimized laser energy density for $(Nd,Sr)NiO_3$ film might show some variation for groups with different PLD systems. We propose that the details of the plume dynamics for $(Nd,Sr)NiO_3$ condensate and laser-target interaction during PLD process deserve further in-depth and systematical study by state-of-art *in-situ* ultrafast imaging and spectroscopic techniques [59, 60].

To further verify the aforementioned mechanism, we also change another growth condition, i.e., the substrate growth temperature, to explore its impact on the film growth. We chose the temperature variation of 570–650 °C (wide enough range to cover most of perovskite oxide epitaxy), while keeping laser energy density of 1.1 $J \cdot cm^{-2}$ and other parameters (oxygen partial pressure, film thickness, reduction temperature and time, etc.) constant. Figures 4(a) and (b) show the XRD scans for the $Nd_{0.8}Sr_{0.2}NiO_3$ precursor films. Note the growth temperature window for perovskite film is relatively wide as (001)/(002) peaks for all the films remain at the same position. The XRD patterns of films after CaH_2 reduction are shown in Figs. 4(c) and (d). All films after reduction show the $Nd_{0.8}Sr_{0.2}NiO_2$ infinite-layer structure. Note that the film grown at 650 °C shows weaker diffraction peaks after reduction, indicating poor film quality due to higher growth temperature. These data illustrate that $Nd_{0.8}Sr_{0.2}NiO_3$ has a wide growth window on substrate temperature, but high temperature growth leads to poor quality for the reduced infinite-layer films. This can also be rationalized from the aforementioned plume dynamics perspective. After laser ablation, the laser-induced plume condensate escapes from the target surface and travels through towards substrate. The momentum and energy of the constitutes in the plume condensate are mainly determined by laser ablation and oxygen molecular scatter, and the substrate surface temperature only plays minimal effect. Therefore, the angular distribution of the plume condensate and the perovskite film growth will not be significantly impact by the substrate temperature.

Although the formation of perovskite and infinite-layer structure seems to be insensitive to the substrate temperature, it does significantly impact the electrical properties. Figure 5(a) shows the temperature dependent resistivity for the $Nd_{0.8}Sr_{0.2}NiO_2$ films (growth temperature of 570–650 °C). Except the highest growth temperature,

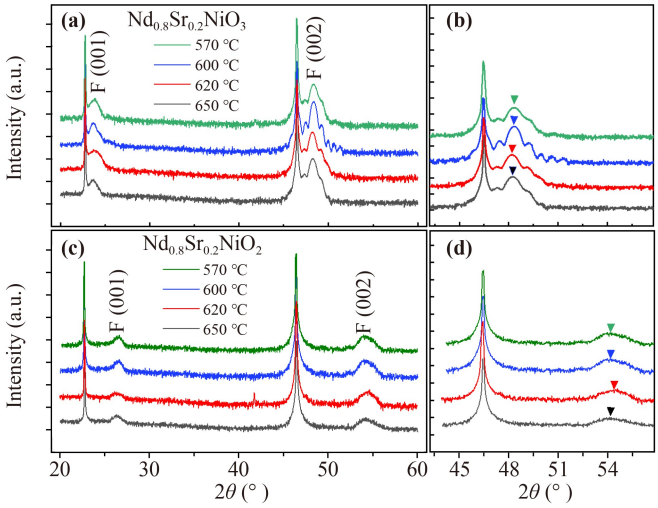

Fig. 4 Effect of substrate temperature on the structural characteristics of nickelate thin films. **(a)** XRD patterns of 15-nm-thick $Nd_{0.8}Sr_{0.2}NiO_3$ (001) films grown on single-crystal $SrTiO_3$ (001) substrates in the temperature range of 570–650 °C and **(b)** the zoomed-in view. **(c)** XRD patterns of 15-nm-thick $Nd_{0.8}Sr_{0.2}NiO_2$ (001) films after reduction correspond in the temperature range of 570–650 °C and **(d)** the zoomed-in view.

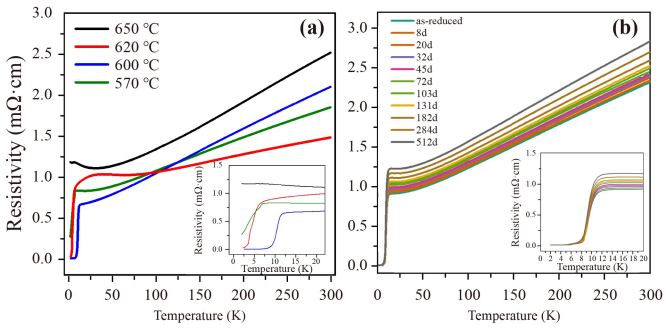

Fig. 5 Effect of substrate temperature on the electrical properties of nickelate thin films and superconductivity stability. **(a)** Temperature-dependent resistivity of $Nd_{0.8}Sr_{0.2}NiO_2$ films grown in the temperature range of 570–650 °C. The inset shows the zoomed-in superconducting transition temperature. **(b)** Temperature dependence of resistivity for superconducting $Nd_{0.8}Sr_{0.2}NiO_2$ films continuously exposed to air for 512 days, the inset shows the superconducting transition temperature for (b) plot.

all other films show superconducting transition with clear resistance drop. At the optimized temperature (600 °C), the $Nd_{0.8}Sr_{0.2}NiO_2$ film shows ideal zero-resistance while at higher or low temperatures (570 and 620 °C) it cannot achieve the zero-resistance state but still shows distinctive superconducting transition. However, at the highest temperature (650 °C), the film does not show any sign of superconducting transition, instead it shows a Kondo-like resistance upturn at 20 K, indicating metal-insulator transition. Since defective secondary phase, i.e., reduced Ruddlesden–Popper inclusions, can still exist in the infinite-layer $Nd_{0.8}Sr_{0.2}NiO_2$ film after reduction [7, 33], the observed nonideal electrical properties at the non-optimized growth temperature can be attributed to these defect phase that compete with the ideal superconducting phase. This is also consistent with the XRD data in Fig. 4(c) that only the film grown at the optimized temperature of 600 °C shows the highest diffraction intensity, while other films show suppressed diffraction intensity, indicating the existence of reduced Ruddlesden –Popper defective phase.

Finally, we show the superconducting $Nd_{0.8}Sr_{0.2}NiO_2$ film grown at the optimized laser energy density and substrate temperature demonstrate excellent environmental stability even without a $SrTiO_3$ caping layer. As we had reported that the superconducting state of $Nd_{0.8}Sr_{0.2}NiO_2$ film can be destroyed by water [36], so it is important that storage condition should be water-free. Once the superconducting $Nd_{0.8}Sr_{0.2}NiO_2$ film is synthesized, it is just stored in a simple Teflon sample box in conventional dry air condition (at room temperature and 35% relative humidity) without glove box protection. Figure 5(b) shows temperature dependent resistivity of the $Nd_{0.8}Sr_{0.2}NiO_2$ film as a function of storage time. While the film shows a slight increase of the normal-state resistance above 14 K (due to the surface absorbance caused by air exposure), the superconducting state and T_c are not affected for 512 days of continuous air exposure. This result clear demonstrates the superconducting $Nd_{0.8}Sr_{0.2}NiO_2$ film can be very robust which is critical for future electronics and device applications.

3 Conclusion

We have systematically investigated the film growth process towards achieving superconducting infinite-layer nickelate $Nd_{0.8}Sr_{0.2}NiO_2$ epitaxial film by PLD. We find the challenges for obtaining superconducting nickelates involve two key aspects. One is to obtain infinite-layer crystal structure and the other is to achieve ideal superconducting state. Due to relatively low formation energy of the Ruddlesden–Popper defective phase, it competes the perovskite phase $Nd_{0.8}Sr_{0.2}NiO_3$. Inequivalent angular distributions of plume condensate for $Nd_{0.8}Sr_{0.2}NiO_3$ target during laser ablation making laser energy density to be very critical to stabilize phase-pure perovskite precursor, which is prerequisite for the formation of infinite-layer structure. We also found both laser energy density and substrate temperature are important for obtaining ideal superconducting state. At the optimized growth conditions, the superconducting $Nd_{0.8}Sr_{0.2}NiO_2$ film can be obtained sustainably. We also demonstrate that superconducting $Nd_{0.8}Sr_{0.2}NiO_2$ film can be very stable in dry air conditions up to 512 days. These results provide important information for the development of the field and for promoting further research on funda-

mental science and device applications of nickelate superconductors.

4 Methods

Film synthesis. The perovskite $Nd_{0.8}Sr_{0.2}NiO_3$ epitaxial films were grown on single-crystal $SrTiO_3$ (001) substrates using pulsed laser deposition (PLD, Demcon TSST) with a KrF excimer laser (λ = 248 nm). As-received $SrTiO_3$ (001) substrates (from HeFeiKeJing Mater. Ltd.) were etched by HF and annealed at 1050 °C for 2 h to achieve atomic-flat TiO_2-termination [61, 62]. The obtained 5 mm × 5 mm size TiO_2-terminated $SrTiO_3$ (001) substrates were then pre-annealed in PLD chamber for 1 h at 640 °C and oxygen partial pressure about 5×10^{-6} Torr to obtain sharp steps before film growth. In this study, we performed ablation using uniform rectangular laser spots size of 1.0 mm × 3 mm, which were formed by aperture imaging. The polycrystalline target $Nd_{0.8}Sr_{0.2}NiO_3$ (synthesized by solid-state reaction method from commercial oxide powders of Nd_2O_3, $SrCO_3$, Ni_2O_3 with stoichiometric ratios) were ablated using laser energy density in the range of 1.0–1.3 J·cm^{-2} with a frequency of 4 Hz. High-pressure *in-situ* reflective high-energy electron diffraction (RHEED, Staib Instruments) was used to monitor the film growth process. In addition, the growth temperature of the perovskite precursor films was set to 550–650 °C and the oxygen partial pressure was kept at 200 mTorr. The temperature rises and falls rate of films is strictly controlled at 10 K/min. All samples mentioned in the text were grown without $SrTiO_3$ capping layer [36].

Topotactic reduction. The as-grown film is loosely wrapped in aluminum foil to avoid direct contact with the reducing agent, placed in a Pyrex glass tube containing 0.1 g CaH_2 powder and vacuum sealed (pressure < 0.1 mTorr). The topotactic reduction was performed at the optimized conditions based on our previous studies [36], i.e., at the temperature of 300 °C and reduction time period of 2 h with the rate of temperature rise and fall fixed at 10 °C·min^{-1}. For air stability test, the as-synthesis superconducting film was stored in vacuum condition right after the structural and electrical measurements.

Structural characterization and transport measurements. The crystal structures of both the as-grown and reduced films were analyzed by high-resolution X-ray diffraction (XRD) and reciprocal space mapping (RSM) using a Bruker D8 Discover diffractometer with a LYNXEYE-2 line detector. A four-bounce double-crystal Ge (220) and a Cu X-ray mirror were placed in the incident beam path to generate monochromatic Cu-Kα X-rays with a beam divergence of 12 arc seconds and the diffracted beam was filtered through a 0.09° parallel plate collimator. Film thickness was determined from X-ray reflectivity (XRR) measurement with an air/film/substrate model simulation. The surface morphology and step-terrace structure of the grown nickelate films were characterized by atomic force microscopy (AFM, Park system, NX10). The temperature dependent (down to 1.6 K) electrical resistivity and Hall effect (up to 9 T magnetic field) of the films were measured by the cryogenic magnet-free system (CFMS, Cryogenics Ltd.) using the four-probe method and the Van der Pauw geometry. Electrical contact of Al wires was bond on deposited Au pads on the film surface by ultrasonic wire bonder.

Declarations The authors declare that they have no competing interests and there are no conflicts.

Author contributions L. Q. conceived the idea and supervised the project. M. H. X and Y. Z synthesized the perovskite nickelate thin films and performed the topotactic reduction experiments. M. H. X., X. D. and S. Z. characterized the crystalline structure. M. H. X., Y. Z., J. G. performed the transport measurements with the help of H. Q. L. and X. D.. M. H. X., Y. Z. and X. D. analyzed the transport data. M. H. X., Y. Z. and L. Q. wrote the manuscript with input from all authors.

Data availability The data that support the findings of this study are available from the corresponding author on reasonable request.

Acknowledgements L. Q. acknowledges the support by the National Natural Science Foundation of China (Grant Nos. 12274061, 52072059, and 11774044), the Science and Technology Department of Sichuan Province (Grant Nos. 2021JDJQ0015 and 2022ZYD0014). B. H. acknowledges the support by the National Natural Science Foundation of China (No. 2230402).

References

1. V. I. Anisimov, D. R. Bukhvalov, and T. M. Rice, Electronic structure of possible nickelate analogs to the cuprates, *Phys. Rev. B* 59(12), 7901 (1999)
2. D. Li, K. Lee, B. Y. Wang, M. Osada, S. Crossley, H. R. Lee, Y. Cui, Y. Hikita, and H. Y. Hwang, Superconductivity in an infinite-layer nickelate, *Nature* 572(7771), 624 (2019)
3. S. Zeng, C. S. Tang, X. Yin, C. J. Li, M. S. Li, Z. Huang, J. X. Hu, D. Y. Wan, P. Yang, S. J. Pennycook, A. T. S. Wee, and A. Ariando, Phase diagram and superconducting dome of infinite-layer thin films, *Phys. Rev. Lett.* 125(14), 147003 (2020)
4. D. Li, B. Y. Wang, K. Lee, S. P. Harvey, M. Osada, B. H. Goodge, L. F. Kourkoutis, and H. Y. Hwang, Superconducting dome in $Nd_{1-x}Sr_xNiO_2$ infinite layer films, *Phys. Rev. Lett.* 125(2), 027001 (2020)
5. W. Sun, Y. Li, R. Liu, J. F. Yang, J. Y. Li, S. J. Yan, H. Y. Sun, W. Guo, Z. B. Gu, Y. Deng, X. F. Wang, and Y. F. Nie, Evidence for quasi-two-dimensional superconductivity in infinite-layer nickelates, *Adv. Mater.* 35(32), 2303400 (2023)
6. P. Werner and S. Hoshino, Nickelate superconductors:

Multiorbital nature and spin freezing, *Phys. Rev. B* 101(4), 041104 (2020)
7. B. Y. Wang, D. Li, B. H. Goodge, K. Lee, M. Osada, S. P. Harvey, L. F. Kourkoutis, M. R. Beasley, and H. Y. Hwang, Isotropic Pauli-limited superconductivity in the infinite-layer nickelate $Nd_{0.775}Sr_{0.225}NiO_2$, *Nat. Phys.* 17(4), 473 (2021)
8. H. Lu, M. Rossi, A. Nag, M. Osada, D. Li, K. Lee, B. Y. Wang, M. Garcia-Fernandez, S. Agrestini, Z. X. Shen, B. Moritz, T. P. Devereaux, J. Zaanen, H. Y. Hwang, K. J. Zhou, and W. S. Lee, Magnetic excitations in infinite-layer nickelates, *Science* 373(6551), 213 (2021)
9. Y. Gu, S. Zhu, X. Wang, J. P. Hu, and H. H. Chen, A substantial hybridization between correlated Ni-d orbital and itinerant electrons in infinite-layer nickelates, *Commun. Phys.* 3(1), 84 (2020)
10. M. Rossi, M. Osada, J. Choi, S. Agrestini, D. Jost, Y. Lee, H. Y. Lu, B. Y. Wang, K. Lee, A. Nag, Y. D. Chuang, C. T. Kuo, S. J. Lee, B. Moritz, T. P. Devereaux, Z. X. Shen, J. S. Lee, K. J. Zhou, H. Y. Hwang, and W. S. Lee, A broken translational symmetry state in an infinite-layer nickelate, *Nat. Phys.* 18(8), 869 (2022)
11. C. C. Tam, J. Choi, X. Ding, S. Agrestini, A. Nag, M. Wu, B. Huang, H. Q. Luo, P. Gao, M. Garcia-Fernandez, L. Qiao, and K. J. Zhou, Charge density waves in infinite-layer $NdNiO_2$ nickelates, *Nat. Mater.* 21(10), 1116 (2022)
12. L. E. Chow, Y. Pierre, M. Nardone, A. Zitouni, A. Goiran, M. S. K. Goh, W. Escoffier, and A. Ariando, Pauli-limit violation in lanthanide infinite-layer nickelate superconductors, arXiv: 2204.12606 (2022)
13. G. Krieger, M. L. Zeng, S. Chow, L. E. Kummer, K. Arpaia, R. Sala, M. M. Brookes, N. B. Ariando, A. Viart, N. Salluzzo, and M. Ghiringhelli, Charge and spin order dichotomy in $NdNiO_2$ driven by the capping layer, *Phys. Rev. Lett.* 129(2), 027002 (2022)
14. D. Zhao, Y. B. Zhou, Y. Fu, L. Wang, X. F. Zhou, H. Cheng, J. Li, D. W. Song, Z. M. Wu, M. Shan, F. H. Yu, J. J. Ying, S. M. Wang, J. W. Mei, T. Wu, and X. H. Chen, Intrinsic spin susceptibility and pseudogaplike behavior in infinite-layer $LaNiO_2$, *Phys. Rev. Lett.* 126(19), 197001 (2021)
15. X. Zhou, X. Zhang, J. Yi, P. X. Qin, Z. X. Feng, P. H. Jiang, Z. C. Zhong, H. Yan, X. N. Wang, H. Y. Chen, H. J. Wu, X. Zhang, Z. A. Meng, X. J. Yu, M. B. H. Breese, J. F. Cao, J. M. Wang, C. B. Jiang, and Z. Q. Liu, Antiferromagnetism in Ni-based superconductors, *Adv. Mater.* 34(4), 2106117 (2022)
16. Y. Cui, C. Li, Q. Li, X. Y. Zhu, Z. Hu, Y. F. Yang, J. S. Zhang, R. Yu, H. H. Wen, and W. Q. Yu, NMR evidence of antiferromagnetic spin fluctuations in $Nd_{0.85}Sr_{0.15}NiO_2$, *Chin. Phys. Lett.* 38(6), 067401 (2021)
17. S. P. Harvey, B. Y. Wang, J. Fowlie, M. Osada, D. Li, and H. Y. Hwang, Evidence for nodal superconductivity in infinite-layer nickelates, arXiv: 2201.12971 (2022)
18. L. E. Chow, S. K. Sudheesh, P. Nandi, E. Zeng, M. Chia, and A. Ariando, Pairing symmetry in infinite-layer nickelate superconductor, arXiv: 2201.10038 (2022)
19. G. M. Zhang, Y. F. Yang, and F. C. Zhang, Self-doped Mott insulator for parent compounds of nickelate superconductors, *Phys. Rev. B* 101(2), 020501 (2020)
20. Q. Gu, Y. Li, S. Wan, H. Z. Li, W. Guo, H. Yang, Q. Li, X. Y. Zhu, X. Q. Pan, Y. F. Nie, and H. H. Wen, Single particle tunneling spectrum of superconducting $Nd_{1-x}Sr_xNiO_2$ thin films, *Nat. Commun.* 11(1), 6027 (2020)
21. Q. Li, C. P. He, J. Si, and H. H. Wen, Absence of superconductivity in bulk $Nd_{1-x}Sr_xNiO_2$, *Commun. Mater.* 1, 16 (2020)
22. M. A. Hayward and M. J. Rosseinsky, Synthesis of the infinite layer Ni(I) phase $NdNiO_{2+x}$ by low temperature reduction of $NdNiO_3$ with sodium hydride, *Solid State Sci.* 5(6), 839 (2003)
23. M. A. Hayward, M. A. Green, M. J. Rosseinsky, and J. Sloan, Sodium hydride as a powerful reducing agent for topotactic oxide deintercalation: Synthesis and characterization of the nickel(I) oxide $LaNiO_2$, *J. Am. Chem. Soc.* 121(38), 8843 (1999)
24. M. Kawai, S. Inoue, M. Mizumaki, N. Kawamura, N. Ichikawa, and Y. Shimakawa, Reversible changes of epitaxial thin films from perovskite $LaNiO_3$ to infinite-layer structure $LaNiO_2$, *Appl. Phys. Lett.* 94(8), 082102 (2009)
25. Y. Tsujimoto, C. Tassel, N. Hayashi, T. Watanabe, H. Kageyama, K. Yoshimura, M. Takano, M. Ceretti, C. Ritter, and W. Paulus, Infinite-layer iron oxide with a square-planar coordination, *Nature* 450(7172), 1062 (2007)
26. T. Katayama, A. Chikamatsu, K. Yamada, K. Shigematsu, T. Onozuka, M. Minohara, H. Kumigashira, E. Ikenaga, and T. Hasegawa, Epitaxial growth and electronic structure of oxyhydride $SrVO_2H$ thin films, *J. Appl. Phys.* 120(8), 085305 (2016)
27. M. Amano Patino, D. Zeng, S. J. Blundell, J. E. McGrady, and M. A. Hayward, Extreme sensitivity of a topochemical reaction to cation substitution: $SrVO_2H$ versus $SrV_{1-x}Ti_xO_{1.5}H_{1.5}$, *Inorg. Chem.* 57(5), 2890 (2018)
28. S. Inoue, M. Kawai, N. Ichikawa, H. Kageyama, W. Paulus, and Y. Shimakawa, Anisotropic oxygen diffusion at low temperature in perovskite-structure iron oxides, *Nat. Chem.* 2(3), 213 (2010)
29. R. M. Helps, N. H. Rees, and M. A. Hayward, $Sr_3Co_2O_{4.33}H_{0.84}$: An extended transition metal oxide-hydride, *Inorg. Chem.* 49(23), 11062 (2010)
30. T. Hanna, Y. Muraba, S. Matsuishi, N. Igawa, K. Kodama, S. Shamoto, and H. Hosono, Hydrogen in layered iron arsenides: Indirect electron doping to induce superconductivity, *Phys. Rev. B* 84(2), 024521 (2011)
31. E. Dixon and M. A. Hayward, The topotactic reduction of $Sr_3Fe_2O_5Cl_2$ — Square planar Fe(II) in an extended oxyhalide, *Inorg. Chem.* 49(20), 9649 (2010)
32. M. A. Hayward, E. J. Cussen, J. B. Claridge, M. Bieringer, M. J. Rosseinsky, C. J. Kiely, S. J. Blundell, I. M. Marshall, and F. L. Pratt, The hydride anion in an extended transition metal oxide array: $LaSrCoO_3H_{0.7}$, *Science* 295(5561), 1882
33. K. Lee, B. H. Goodge, D. Li, M. Osada, B. Y. Wang, Y. Cui, L. F. Kourkoutis, and H. Y. Hwang, Aspects of the synthesis of thin film superconducting infinite-layer nickelates, *APL Mater.* 8(4), 041107 (2020)

34. A. Olafsen, H. Fjellvåg, and B. C. Hauback, Crystal Structure and Properties of $Nd_4Co_3O_{10+\delta}$ and $Nd_4Ni_3O_{10-\delta}$, *J. Solid State Chem.* 151(1), 46 (2000)
35. Q. Gao, Y. Zhao, X. J. Zhou, and Z. Zhu, Preparation of superconducting thin films of infinite-layer nickelate, *Chin. Phys. Lett.* 38(7), 077401 (2021)
36. X. Ding, S. Shen, H. Leng, M. H. Xu, Y. Zhao, J. R. Zhao, X. L. Sui, X. Q. Wu, H. Y. Xiao, X. T. Zu, B. Huang, H. Q. Luo, P. Yu, and L. Qiao, Stability of superconducting $Nd_{0.8}Sr_{0.2}NiO_2$ thin films, *Sci. China Phys. Mech. Astron.* 65(6), 267411 (2022)
37. G. A. Pan, D. Ferenc Segedin, H. LaBollita, Q. Song, E. M. Nica, B. H. Goodge, A. T. Pierce, S. Doyle, S. Novakov, D. Córdova Carrizales, A. T. N'Diaye, P. Shafer, H. Paik, J. T. Heron, J. A. Mason, A. Yacoby, L. F. Kourkoutis, O. Erten, C. M. Brooks, A. S. Botana, and J. A. Mundy, Superconductivity in a quintuple-layer square-planar nickelate, *Nat. Mater.* 21(2), 160 (2022)
38. Y. Y. Ji, J. H. Liu, X. F. Gao, L. Li, K. Chen, and Z. L. Liao, Optimized fabrication of high-quality $N_{0.8}Sr_{0.2}NiO_2$ superconducting films by pulsed laser deposition, *Physica C* 604, 1354190 (2023)
39. A. Ohtomo and H. Y. Hwang, A high-mobility electron gas at the $LaAlO_3/SrTiO_3$ heterointerface, *Nature* 427(6973), 423 (2004)
40. X. C. Huang, W. W. Li, S. Zhang, F. E. Oropeza, G. Gorni, V. A. de la Peña-O'Shea, T. L. Lee, M. Wu, L. S. Wang, D. C. Qi, L. Qiao, J. Cheng, and K. H. L. Zhang, Ni^{3+}-induced semiconductor-to-metal transition in spinel nickel cobaltite thin films, *Phys. Rev. B* 104(12), 125136 (2021)
41. H. M. Christen and G. Eres, Recent advances in pulsed-laser deposition of complex oxides, *J. Phys.: Condens. Matter* 20(26), 264005 (2008)
42. J. D. Haverkamp, M. A. Bourham, S. Du, and J. Narayan, Plasma plume dynamics in magnetically assisted pulsed laser deposition, *J. Phys. D Appl. Phys.* 42(2), 025201 (2009)
43. K. Horiba, R. Eguchi, M. Taguchi, A. Chainani, A. Kikkawa, Y. Senba, H. Ohashi, and S. Shin, Electronic structure of $LaNiO_{3-x}$: An in situ soft X-ray photoemission and absorption study, *Phys. Rev. B* 76(15), 155104 (2007)
44. P. D. C. King, H. I. Wei, Y. F. Nie, M. Uchida, C. Adamo, S. Zhu, X. He, I. Bozovic, D. G. Schlom, and K. M. Shen, Atomic-scale control of competing electronic phases in ultrathin $LaNiO_3$, *Nat. Nanotechnol.* 9(6), 443 (2014)
45. L. Qiao and X. Bi, Direct observation of Ni^{3+} and Ni^{2+} in correlated $LaNiO_{3-\delta}$ films, *Europhys. Lett.* 93(5), 57002 (2011)
46. K. Tsubouchi, I. Ohkubo, H. Kumigashira, Y. Matsumoto, T. Ohnishi, M. Lippmaa, H. Koinuma, and M. Oshima, Epitaxial growth and surface metallic nature of $LaNiO_3$ thin films, *Appl. Phys. Lett.* 92(26), 262109 (2008)
47. S. Middey, J. Chakhalian, P. Mahadevan, J. W. Freeland, A. J. Millis, and D. D. Sarma, Physics of ultrathin films and heterostructures of rare-earth nickelates, *Annu. Rev. Mater. Res.* 46(1), 305 (2016)
48. J. C. S. Kools, T. S. Baller, S. T. De Zwart, and J. Dieleman, Gas flow dynamics in laser ablation deposition, *J. Appl. Phys.* 71(9), 4547 (1992)
49. A. V. Bulgakov and N. M. Bulgakova, Gas-dynamic effects of the interaction between a pulsed laser-ablation plume and the ambient gas: Analogy with an underexpanded jet, *J. Phys. D Appl. Phys.* 31(6), 693 (1998)
50. I. NoorBatcha, R. R. Lucchese, and Y. Zeiri, Effects of gas-phase collisions on particles rapidly desorbed from surfaces, *Phys. Rev. B* 36(9), 4978 (1987)
51. J. C. S. Kools, E. van de Riet, and J. Dieleman, A simple formalism for the prediction of angular distributions in laser ablation deposition, *Jpn. J. Appl. Phys.* 69(1–4), 133 (1993)
52. T. C. Droubay, L. Qiao, T. C. Kaspar, M. H. Engelhard, V. Shutthanandan, and S. A. Chambers, Nonstoichiometric material transfer in the pulsed laser deposition of $LaAlO_3$, *Appl. Phys. Lett.* 97(12), 124105 (2010)
53. L. Qiao, T. C. Droubay, V. Shutthanandan, Z. Zhu, P. V. Sushko, and S. A. Chambers, Thermodynamic instability at the stoichiometric $LaAlO_3/SrTiO_3$ (001) interface, *J. Phys.: Condens. Matter* 22(31), 312201 (2010)
54. R. E. Muenchausen, K. M. Hubbard, S. Foltyn, R. C. Estler, N. S. Nogar, and C. Jenkins, Effects of beam parameters on excimer laser deposition of $YBa_2Cu_3O_{7-\delta}$, *Appl. Phys. Lett.* 56(6), 578 (1990)
55. T. Ohnishi, K. Shibuya, T. Yamamoto, and M. Lippmaa, Defects and transport in complex oxide thin films, *J. Appl. Phys.* 103(10), 103703 (2008)
56. I. Konomi, T. Motohiro, M. Horii, and M. Kawasumi, Angular distribution of elemental composition of films deposited by laser ablation of a $SrZrO_3$ target, *J. Vac. Sci. Technol. A* 26(6), 1455 (2008)
57. H. Dang and Q. Qin, Angular distribution of laser-ablated species from a $Pr_{0.67}Sr_{0.33}MnO_3$ target, *Phys. Rev. B* 60(15), 11187 (1999)
58. M. Tyunina, J. Levoska, and S. Leppävuori, Experimental studies and modeling of Pb–Zr–Ti–O film growth in pulsed laser deposition, *J. Appl. Phys.* 83(10), 5489 (1998)
59. R. F. Wood, K. R. Chen, J. N. Leboeuf, A. A. Puretzky, and D. B. Geohegan, Dynamics of plume propagation and splitting during pulsed-laser ablation, *Phys. Rev. Lett.* 79(8), 1571 (1997)
60. D. B. Geohegan, Fast intensified-CCD photography of $YBa_2Cu_3O_{7-x}$ laser ablation in vacuum and ambient oxygen, *Appl. Phys. Lett.* 60(22), 2732 (1992)
61. X. Ding, B. Yang, H. Leng, J. H. Jang, J. R. Zhao, C. Zhang, S. Zhang, G. X. Cao, J. Zhang, R. Mishra, J. B. Yi, D. Qi, Z. Gai, X. Zu, S. Li, B. Huang, A. Borisevich, and L. Qiao, Crystal symmetry engineering in epitaxial perovskite superlattices, *Adv. Funct. Mater.* 31(47), 2106466 (2021)
62. L. Qiao, K. H. L. Zhang, M. E. Bowden, T. Varga, V. Shutthanandan, R. Colby, Y. Du, B. Kabius, P. V. Sushko, M. D. Biegalski, and S. A. Chambers, The impacts of cation stoichiometry and substrate surface quality on nucleation, structure, defect formation, and intermixing in complex oxide heteroepitaxy–$LaCrO_3$ on $SrTiO_3$(001), *Adv. Funct. Mater.* 23(23), 2953 (2013)